Resource

Cell Host & Microbe

Temporal Landscape of MicroRNA-Mediated Host-Virus Crosstalk during Productive Human Cytomegalovirus Infection

Graphical Abstract

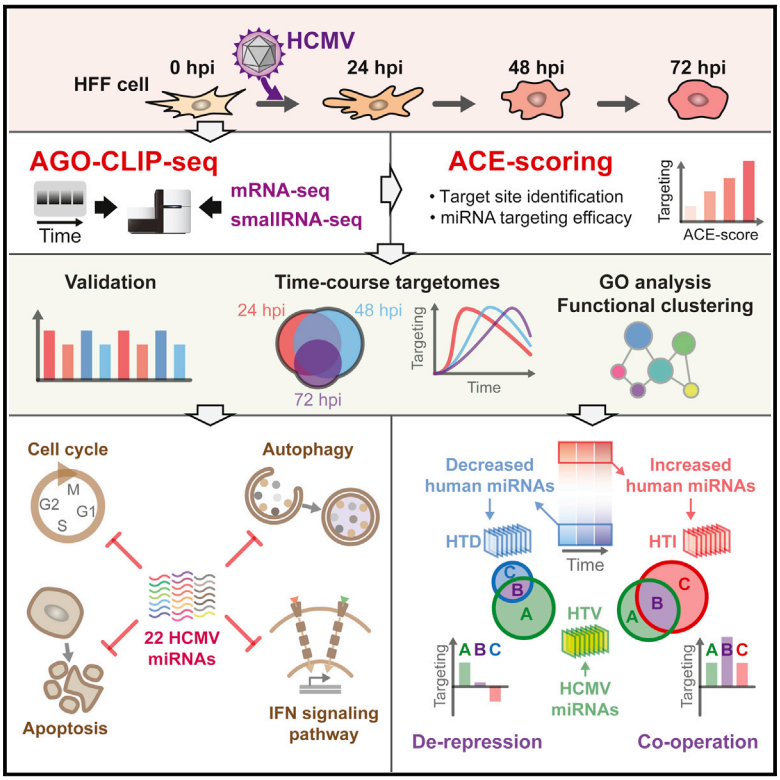

Highlights

- ACE-scoring method based on AGO-CLIP-seq quantifies the repression at miRNA target sites
- Global temporal HCMV miRNA targetomes during lytic HCMV infection are reported
- HCMV miRNAs function in cellular processes central for HCMV virology
- HCMV miRNAs utilize host miRNAs with intimate cooperation and co-targeting

Authors

Sungchul Kim, Daekwan Seo, Dongwoo Kim, ..., V. Narry Kim, Sungwook Lee, Kwangseog Ahn

Correspondence

ksahn@snu.ac.kr

In Brief

Kim et al. use AGO-CLIP-seq combined with a bioinformatic ACE-scoring method to describe temporal miRNA targetomes during productive HCMV infection. This holistic survey reveals that HCMV miRNAs can regulate multiple pathways central for HCMV biology and cooperatively function with human miRNAs, providing a valuable resource for understanding host-virus interactions.

Accession Numbers

GSE63797

Kim et al., 2015, Cell Host & Microbe *17*, 838–851
June 10, 2015
http://dx.doi.org/10.1016/j.chom.2015.05.014

CellPress

Cell Host & Microbe
Resource

Temporal Landscape of MicroRNA-Mediated Host-Virus Crosstalk during Productive Human Cytomegalovirus Infection

Sungchul Kim,[1,2,5] Daekwan Seo,[1,2,5] Dongwoo Kim,[2] Yujin Hong,[1,2] Hyeshik Chang,[1,2] Daehyun Baek,[1,2,3] V. Narry Kim,[1,2] Sungwook Lee,[4] and Kwangseog Ahn[1,2,*]

[1]Center for RNA Research, Institute for Basic Science (IBS), Seoul 151-742, Korea
[2]School for Biological Sciences, Seoul National University (SNU), Seoul 151-742, Korea
[3]Bioinformatics Institute, Seoul National University, Seoul 151-747, Republic of Korea
[4]Department of Systems Biology, Yonsei University, Seoul 120-749, Korea
[5]Co-first author
*Correspondence: ksahn@snu.ac.kr
http://dx.doi.org/10.1016/j.chom.2015.05.014

SUMMARY

Temporal profiles of miRNA activity during productive virus infection can provide fundamental insights into host-virus interactions. Most reported miRNA targetome analyses in the context of virus infection have been performed in latently infected cells and lack reliable models for quantifying the suppression efficacy at specific miRNA target sites. Here, we identified highly competent temporal miRNA targetomes during lytic HCMV infection by using AGO-CLIP-seq together with a bioinformatic method that quantifies miRNA functionality at a specific target site, called ACE-scoring. The repression efficiency at target sites correlates with the magnitude of the ACE-score, and temporal HCMV-encoded miRNA targetomes identified by ACE-scoring were significantly enriched in functional categories involved in pathways central for HCMV biology. Furthermore, comparative analysis between human and viral miRNA targetomes supports the existence of intimate cooperation and co-targeting between them. Our holistic survey provides a valuable resource for understanding host-virus interactions during lytic HCMV infection.

INTRODUCTION

Since the first report of viral miRNAs in 2004 (Pfeffer et al., 2004), numerous viral miRNAs have been discovered, mainly in herpesviruses (Kincaid and Sullivan, 2012). To date, at least 22 miRNAs encoded by human cytomegalovirus (HCMV), a β-herpesvirus, have been identified from 12 pre-miRNAs (Stark et al., 2012). Most target search studies of HCMV-encoded miRNAs have been performed at the single miRNA-single target interaction level or by narrow-range screening methods (Hook et al., 2014a), necessitating a more accurate genome-wide targetome analysis during HCMV infection.

Although bioinformatic prediction algorithms have played valuable roles in the discovery of new miRNA targets, current algorithms have high false positive or negative rates (Thomson et al., 2011). Thus, the genome-wide identification of authentic miRNA-target interactions requires a combination of sophisticated biochemical approaches and bioinformatics analysis. To this end, argonaute-crosslinking and immunoprecipitation followed by high-throughput sequencing (AGO-CLIP-seq, also known as Ago HITS-CLIP) methods have been developed to overcome insufficient in silico prediction of miRNA-target interaction sites (Chi et al., 2009). AGO-CLIP-seq methods provide significantly higher resolution data regarding the precise location of binding sites, avoiding the potential limitations of miRNA-target search methods based on mRNA expression profiling and proteomics techniques.

Several groups have successfully adopted the AGO-CLIP-seq method to identify targets of Epstein-Barr virus (EBV) miRNAs and Kaposi's sarcoma-associated herpesvirus (KSHV) miRNAs in the latently infected cell lines with γ-herpesviruses (Gottwein et al., 2011; Haecker et al., 2012; Riley et al., 2012; Skalsky et al., 2012). However, there have been no temporal investigations for the miRNA targetomes during productive infection of miRNA-encoding viruses, including HCMV.

In this study, we describe the application of an AGO-CLIP-seq-based approach to characterize the global miRNA targetome during productive HCMV infection. We also developed a bioinformatic quantitation method, ACE-scoring (AGO-CLIP-seq enrichment scoring), to accurately identify miRNA target sites and calculate the targeting efficacy of miRNA-target interactions. We collectively discovered and validated the functionality of miRNA-target interactions and their correlation with calculated ACE-scores. We observed and verified various target genes in cellular pathways important for HCMV infection progression. In addition, comparative analysis between human miRNA and HCMV miRNA targetomes revealed functional relationships by co-targeting and cooperation. Our quantitative temporal data on miRNA targetomes provide a key foothold for the study of HCMV virology, facilitating the detailed analysis of and further insight into viral pathogenesis and novel drug discovery.

RESULTS

Temporal Features of AGO-CLIP-Seq, mRNA-Seq, and smallRNA-Seq during Lytic HCMV Infection

To analyze the targetome in HCMV-infected cells, we performed AGO-CLIP-seq in triplicate and both mRNA-seq and smallRNA-seq in duplicate with human foreskin fibroblasts (HFFs) uninfected or infected with HCMV $Towne_{long}$ and harvested at 0 (uninfected), 24, 48, and 72 hr after infection (Figure 1A). The expression of phase marker genes and cell viability were confirmed (Figures 1B and S1A, available online). To exclude bias in targetome identification from differential AGO IP efficiency of viral miRNAs, we used the pan-AGO-specific mouse monoclonal antibody 2A8 (Nelson et al., 2007), which can capture all human AGO proteins (hAGO1–4; Figure S1B). From purified UV-crosslinked radioactive AGO-RNA complexes (Figure 1B), CLIPed RNA-3′-adaptor species of 40–77 nt were excised, purified, and ligated to a 5′-RNA adaptor and then subjected to RT-PCR (Figure 1C). The amplicon libraries yielded a strong peak at the miRNA or highly digested mRNA-derived band size (136–145 bp) and exhibited several larger RNA-derived species (145–170 bp), consistent with prior reports on CLIP-seq-based AGO-interacting targetome analysis (Chi et al., 2009; Leung et al., 2011; Riley et al., 2012). We also prepared mRNA-seq and smallRNA-seq libraries to assist with the complicated data processing and as controls for the comparative analysis of mRNA or miRNA expression (Figures S1C and S1D).

The sequencing data were processed by pipeline designed in Figure S1E and were sufficient (Table S1A–S1C) and reproducible (Figures S1F and S1G). The majority of the AGO-CLIP-seq reads mapped to human and viral miRNA genomic regions, and 4%–9% mapped to human mRNA genomic regions (Figure 1D), consistent with previous observations in AGO-CLIP-seq-based studies (Leung et al., 2011). The specificity of the AGO-CLIP-seq method was demonstrated by the relative lack of AGO crosslinking to highly abundant rRNAs (3.66%–7.64%) and tRNAs (0.52%–0.76%). Together, the quantity and quality of the AGO-CLIP-seq, mRNA-seq, and smallRNA-seq reads were adequate for further bioinformatic miRNA targetome analysis.

Canonical miRNA target sites are mostly located in the 3′-UTRs of mRNAs rather than the 5′-UTR or CDS regions (Fabian et al., 2010). Although a significant fraction of the AGO-CLIP-seq reads mapped to mRNA CDS regions, consistent with prior reports (Boudreau et al., 2014; Chi et al., 2009; Hafner et al., 2010), reads in the 3′-UTR were enriched 2-fold in AGO-CLIP-seq (approximately 60%) compared to mRNA-seq (approximately 30%) (Figure 1D). Additionally, AGO-CLIP-seq reads near the stop codon were more enriched in the 3′-UTR than in CDS regions; however, there was no differential enrichment between AGO-CLIP-seq and mRNA-seq in the 5′-UTR, and there were more CDS reads around the start and stop codons in mRNA-seq than in AGO-CLIP-seq (Figure 1E). These results suggested that our AGO-CLIP-seq data might contain a considerable proportion of clusters that were crosslinked to AGO proteins together with virtual miRNA target sites in the 3′-UTRs of mRNAs. Thus, we focused on the mRNA 3′ UTR as the major targeting site of viral miRNAs.

Comprehensive Identification of Canonical Human Targets of HCMV miRNAs Using ACE-Scoring

To analyze the human mRNA targetome of HCMV miRNAs, we first characterized the peak clusters of AGO-CLIP-seq reads after Q value correction as an appropriate peak-calling method for the identification of miRNA target sites (Figures S2A–S2C). The observation that the expression of the refined 22 viral miRNAs exponentially increased during infection (Figures S2D and S2E and Table S1D) suggested that the relative intensities of the peak clusters at all the viral miRNA target sites during maximum viral miRNA targeting efficacy should be increased compared to earlier time points. Because the number of total AGO-CLIP-seq reads for each mRNA was generally greater when the mRNA was more highly expressed (Figure S2F), an increase in absolute depth size within a peak cluster at a given time point compared to a previous time point does not simply reflect targeting intensity, suggesting that the fold change in AGO-CLIP-seq reads should be compared to the number of mRNA-seq reads in a peak cluster. We therefore introduced the concept of an "increased AGO-CLIP-seq" constraint as an indicator of miRNA targeting intensity and reported this value as the "ACE-score" (AGO-CLIP-seq enrichment score) (Figures 2A and S2A).

Notably, the ACE-scores of the peak clusters that are actively targeted by viral miRNAs should be positive (ACE-score > 0). Nonetheless, many positive ACE-score peak cluster regions might not be viral miRNA target sites because many human miRNA target sites that show increased expression after infection might have a positive ACE-score. Although some functional non-seed target rules have been reported, we observed that seed-independent target sites were identified at a relatively lower abundance than seed-dependent sites (Table S2A). Moreover, the representation rate of mutation sites in most viral miRNAs in AGO-CLIP-seq reads was enriched in the binding regions of non-seed nucleotides (Figures S2D, S2G, and S2H), indicating that most viral miRNAs might exhibit seed site-mediated target interactions that increase the frequency of UV-crosslinking during the CLIP-seq procedure for miRNA nucleotides, which are not base-paired in AGO-miRNA-mRNA ternary complexes. Therefore, to identify reliable peak clusters targeted by viral miRNAs, we selected peak clusters containing viral miRNA seed binding motifs (6-mer, 7-mer-m8, 7-mer-A1, and 8-mer) (Grimson et al., 2007) with positive ACE-scores. As a result, we collectively identified 3,909 human targets of the viral miRNAs from temporal sets of 2,531 (24 hpi), 2,968 (48 hpi), and 1,394 (72 hpi) genes. We defined the target gene groups containing the seed motif-filtered peak clusters with positive ACE-scores in the 3′ UTR of human mRNA as the canonical human targetome of viral miRNAs (HTV) (Figure 2B and Table S3).

ACE-Score Reflects the Targeting Functionality in HTV

To assess the functionality of the HTV targets, the overall fold changes in mRNA expression of the 3,909 identified HTV targets were compared with the expression fold changes of total mRNAs and/or non-targets. HTV targets were generally suppressed at the mRNA level at 24, 48, and 72 hpi compared to the uninfected control (Figure 2C), and the targeting effects were prolonged during infection (Figure 2D). HTV targets with an ACE-score > 1 were slightly more suppressed than total HTV targets (ACE-score > 0) (Figures 2C and 2D). All the HTV targets of individual

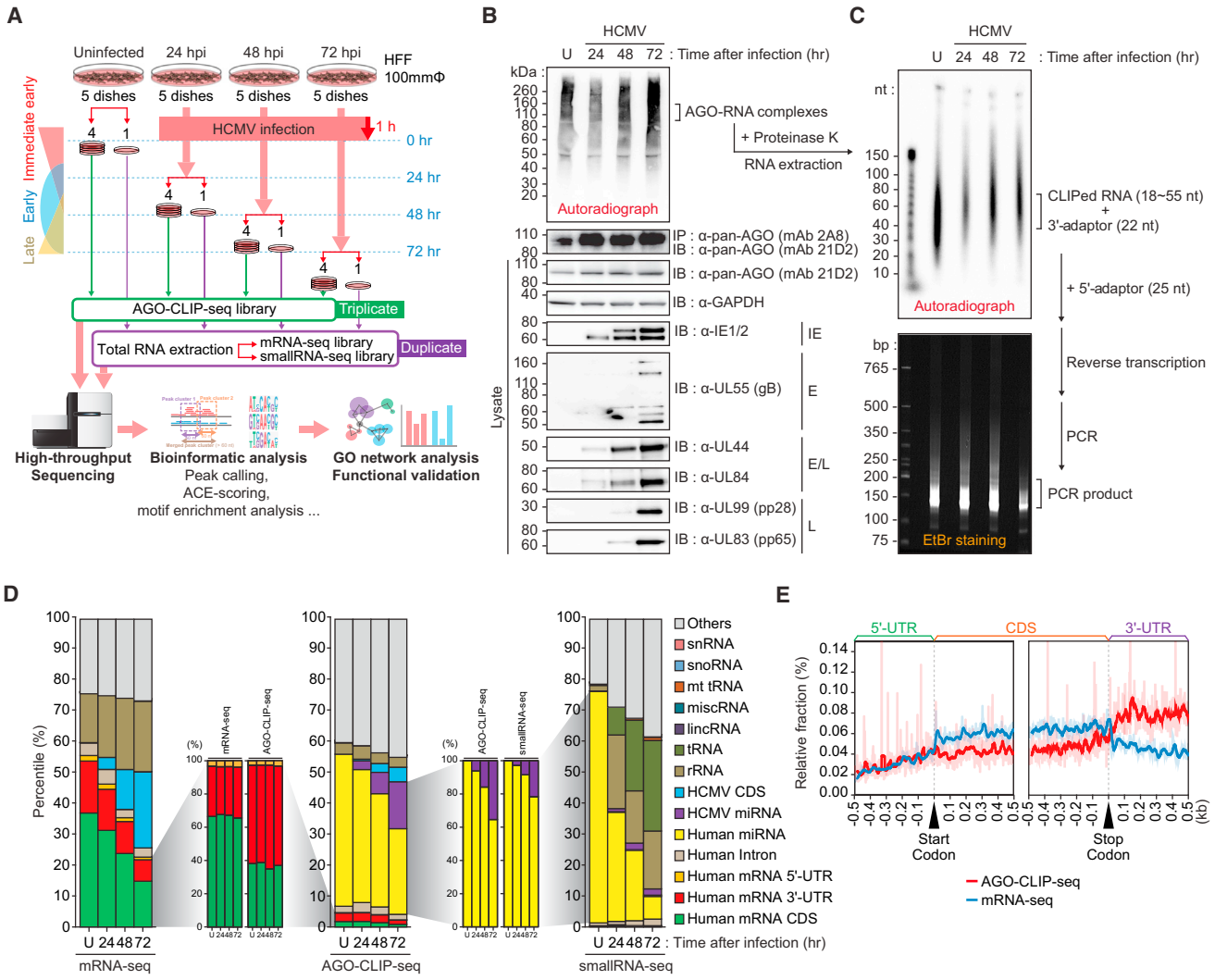

Figure 1. Temporal AGO-CLIP-Seq Analysis in HCMV-Infected Cells

(A) Workflow of AGO-CLIP-seq, mRNA-seq, and smallRNA-seq in the context of HCMV infection.

(B) Representative autoradiography and immunoblots of AGO-CLIPed ^{32}P-labeled RNA-AGO complexes from uninfected or infected HFFs after infection for the indicated times. With aliquots of time point lysates used in AGO-CLIP-seq, immunoblotting was performed with anti-pan-AGO, anti-IE1/2, anti-UL55, anti-UL44, anti-UL84, anti-UL99, anti-UL83, and anti-GAPDH (loading control) antibodies. The expression phases of viral genes are indicated as IE (immediate early), E (early), and L (late).

(C) Top: autoradiograph of the RNA urea-polyacrylamide gel after proteinase K treatment and RNA extraction from the indicated Ago-RNA complex region of the membrane in (B). Bottom: verification of RT-PCR products of 5′- and 3′-adaptor-ligated CLIPed RNAs after proteinase K treatment and RNA extraction from the transferred membrane.

(D) Relative fraction of reads mapped to indicated human or HCMV genomic regions of AGO-CLIP-seq, mRNA-seq, and smallRNA-seq data. snRNA, small nuclear RNA; snoRNA, small nucleolar RNA; mt tRNA, mitochondrial tRNA; miscRNA, miscellaneous RNA; lincRNA, long intergenic non-coding RNA; CDS, coding sequence; UTR, untranslated region. Relative fraction of reads mapped to human or HCMV miRNA-encoding regions of smallRNA-seq and AGO-CLIP-seq data and reads mapped to the indicated regions within human mRNAs of AGO-CLIP-seq data are represented.

(E) Relative fraction of AGO-CLIP-seq and mRNA-seq reads mapped to positions (up to ±500 nt) relative to mRNA start and stop codons. Data are plotted as the normalized density relative to transcript abundance for AGO-CLIP-seq reads (red) or mRNA-seq reads (blue). For each time point, the average value of AGO-CLIP-seq triplicate or mRNA-seq duplicate read counts was calculated at each position. The AGO-CLIP-seq read count average was divided by mRNA-seq read count average. Data are presented as the sum of calculated average counts at all times. The mRNAs for this analysis were calculated with length limits > 500 nt in the 5′ UTR, > 1,000 nt in CDS, and > 500 nt in the 3′ UTR.

See also Figure S1 and Table S1.

viral miRNAs were highly suppressed (Figures S2I and S2J), indicating that all the viral miRNAs were functional during infection.

In determining whether the suppression level corresponded with the ACE-score, we observed that the first quartile of the HTV showed the greatest level of transcriptome suppression, and the degree of suppression sequentially weakened toward the last quartile (Figure 2E). The first quartile of the HTV had the lowest Context+ score (C+ score); this score was developed

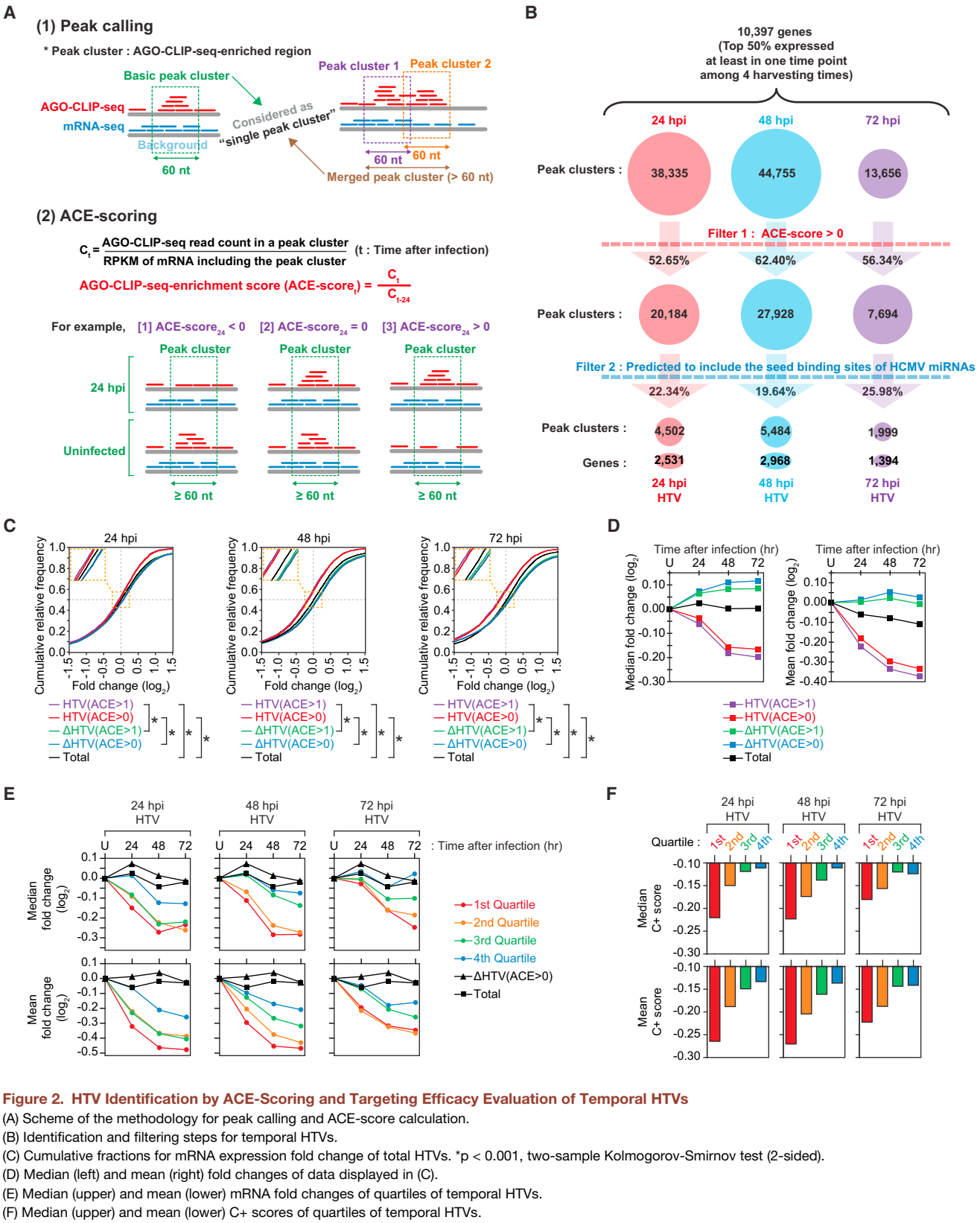

Figure 2. HTV Identification by ACE-Scoring and Targeting Efficacy Evaluation of Temporal HTVs

(A) Scheme of the methodology for peak calling and ACE-score calculation.

(B) Identification and filtering steps for temporal HTVs.

(C) Cumulative fractions for mRNA expression fold change of total HTVs. *p < 0.001, two-sample Kolmogorov-Smirnov test (2-sided).

(D) Median (left) and mean (right) fold changes of data displayed in (C).

(E) Median (upper) and mean (lower) mRNA fold changes of quartiles of temporal HTVs.

(F) Median (upper) and mean (lower) C+ scores of quartiles of temporal HTVs.

See also Figure S2 and Tables S2 and S3.

to calculate the targeting efficiency using multiple features and is considered one of the most powerful algorithms to evaluate miRNA or siRNA targeting efficiency (Garcia et al., 2011). The C+ score sequentially decreased toward the last quartile (Figure 2F). Thus, these results indicated that the target suppression efficacy at the HTV target sites correlated with the magnitude of the ACE-score.

Unbiased sequence motif enrichment analysis is a useful method for analyzing the HTV peak cluster regions to evaluate the likelihood of viral miRNA targeting (Boudreau et al., 2014; Leung et al., 2011; Zhang and Darnell, 2011). Among MEME (multiple EM for motif elicitation) (Bailey and Elkan, 1994) motifs significantly enriched for peak clusters with an ACE-score > 1, we found that 7 of 10 at 24 hpi, 6 of 10 at 48 hpi, and 6 of 10 at 72 hpi corresponded to viral miRNA seed sequences (Table S2B, upper tables). Mutations frequently induced in UV-cross-linked nucleotides during AGO-CLIP-seq have been regarded as important identifiers of reasonable miRNA target sites (Zhang and Darnell, 2011). Crosslinking-induced mutation site (CIMS) analysis of peak clusters can identify the precise interaction sites, and the significance of the sites can be represented by the FDR (false discovery rate). We selected peak sites with a CIMS FDR < 0.05 and performed a MEME analysis of these peak sites. No obvious enrichment of viral and human miRNA target sites was observed (Table S2B, lower tables). This result suggests that although CIMS analysis can be a useful method for evaluating the accuracy of RNA-binding protein interaction sites, it is not adequate for identifying all precise miRNA target sites from genome-wide AGO-CLIP-seq data. Taken together, we concluded that our temporal HTVs sorted by the ACE-scoring method represent virtual target genes of viral miRNAs.

Validation of the Suppression of High-Confidence HTV Targets

To test whether HTV targets were suppressed by the corresponding viral miRNAs, we selected high-confidence candidates from temporal HTVs (Figure S3A and Table S4) and examined the fold reduction in mRNA expression by transfecting the targeting viral miRNAs into HFFs. At 48 hr post-transfection, total RNA was extracted and examined by quantitative real-time PCR (qRT-PCR), which revealed that 26 of 30 mRNAs were significantly downregulated (Figure 3A).

To further investigate whether high-confidence HTV target interactions were mediated by seed binding, we constructed firefly luciferase reporters for either wild-type target 3′ UTR (WT) or seed-mutated target 3′ UTR (Mut) (Figure S3B). Dual luciferase assays were performed, and 26 of 30 miRNA-target mRNA combinations showed decreased luciferase activity in the WT context compared to control miRNA, but the relative luciferase activities of the Mut were comparable with or recovered toward the control miRNA transfections (Figure 3B). These results validated the reliability of high-confidence HTV targets and provided a basis for further functional investigations of our ACE-score-supported HTV targets.

Functional Significance for Sub-temporal HTVs over the Course of Productive Infection

To ascertain more detailed information on the temporal HTVs, we divided the three temporal HTV groups (24 hpi HTV, 48 hpi HTV, and 72 hpi HTV) into seven sub-temporal groups (HTV-E, HTV-EM, HTV-M, HTV-ML, HTV-L, HTV-EL, and HTV-All; E, early; M, mid; L, late) based on overlap among the temporal groups (Figure 4A). The time course comparison analysis of the fold change in the sub-temporal HTVs at the transcriptome level revealed that the repression of earlier sub-temporal HTVs was greatest in the early phase, whereas that of later sub-temporal HTVs was maximal in the late phase (Figure 4B). These results indicated that sub-temporal HTVs might undergo time-dependent target suppression with maximal target suppression efficacy during their representative time points. Because all HCMV miRNAs are increasingly expressed during productive infection (Figure S2E), the target suppression of viral miRNAs might theoretically continue and gradually accumulate during infection. When mRNAs that are transcriptionally induced by infection stimuli are targeted by viral miRNAs, a positive ACE-score can occur at a later phase of infection due to sustained target suppression by increasingly expressed viral miRNAs and on the characteristics of ACE-score calculation. Thus, all sub-temporal HTVs are continually suppressed by viral miRNAs during infection, and maximum target suppression periods might be determined by the inducibility of target transcripts after infection.

To further investigate which factors affect the relatively high propensity toward the upregulation of late time-specific temporal targetomes at the early phase of infection, we hypothesized that genes induced and activated by viral entry and viral gene function at the immediate-early stage might be upstream regulators of the initial induction of late time-specific HTV targets. Therefore, we performed an upstream analysis using ingenuity pathway analysis of 72 hpi HTV genes upregulated at 24 hpi compared to the uninfected state and determined that several genes (*MAPK8*, *PDGFB*, *MAPK1*, *HIF1A*, *JUN*, *CEBPB*, *EGFR*, *TNF*, *CCL5*, *RUVBL1*, *ERG*, *DNMT3B*, *EGF*, and *MYC*) that are known to be activated or induced at the initial stage of HCMV infection were significantly enriched (Figure 4C and Table S5) (Boldogh et al., 1991; Kapoor et al., 2012; McFarlane et al., 2011; Rodems and Spector, 1998; Soroceanu et al., 2008; Wang et al., 2003; Xuan et al., 2009). These results suggested that HCMV miRNAs can regulate the expression of downstream genes, which might be represented in later-phase HTV targets and induced by viral entry stimuli or viral IE gene expression through the early-to-late stages of productive infection in a buffering-like manner.

To determine the functional features of sub-temporal HTVs and all the HTV targets, we performed gene ontology (GO) analysis and network clustering of GO terms using ClueGO, a Cytoscape plug-in software (Bindea et al., 2009), and visualized particularly enriched functional annotation categories as a network (Figures 4D and S4 and Table S6). In agreement with the widespread roles of HTV targets, these enriched terms represent several important aspects of HCMV infection, such as cell-cycle regulation, which is associated with pseudo G1 phase establishment in HCMV infection (Sanchez and Spector, 2008), apoptosis inhibition, which is typically harmful to virus production, autophagy regulation, which is utilized by many viruses to produce viral particles and inhibit anti-viral autophagy mechanisms (Yordy et al., 2013), and secretory pathway consistent with a recent study (Hook et al., 2014b). Therefore, it indicated

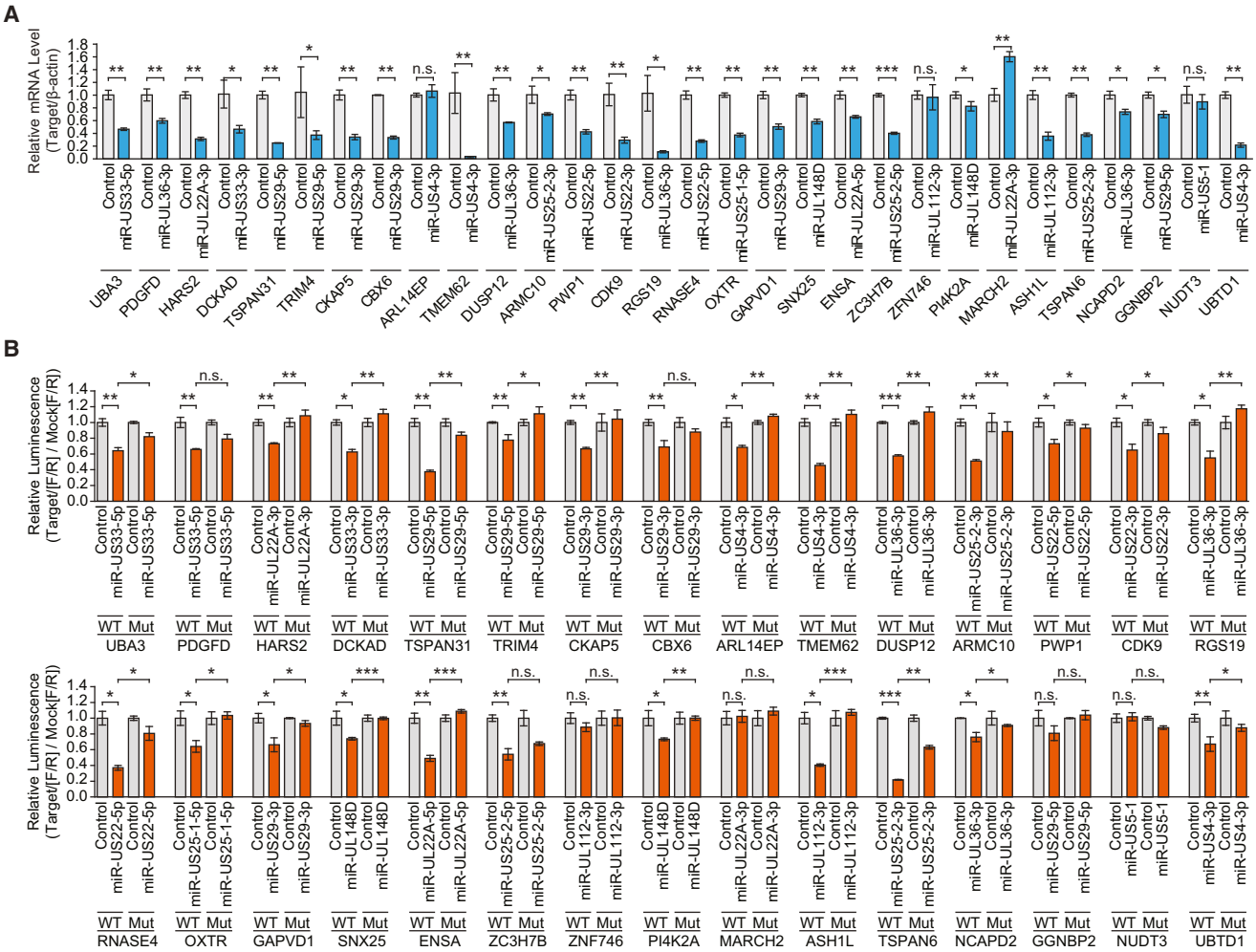

Figure 3. Validation of High-Confidence HTV Targets

(A) Fold changes of mRNAs targeted by corresponding HCMV miRNAs. The expression levels of target mRNAs were analyzed using qRT-PCR. *$p < 0.05$, **$p < 0.01$, ***$p < 0.001$, bootstrapped t test with 10,000 repetitions, compared with control miRNA. Data are presented relative to the value of β-actin as means ± SEM, n = 3.

(B) Relative luminescence of firefly luciferase with wild-type (WT) or seed-mutated (Mut) target 3′ UTRs with corresponding HCMV miRNAs. Dual luciferase assays were performed in HEK293T cells using 20 pmol of miRNA oligomer duplexes, 5 ng of the pDEST-GL3-3′ UTR vector, and 2.5 ng of the *Renilla* control vector in a 24-well format. *$p < 0.05$, **$p < 0.01$, ***$p < 0.001$, bootstrapped t test with 10,000 repetitions, compared with control miRNA. Data are presented by dual normalization (Target[Firefly/*Renilla*] divided by Mock[Firefly/*Renilla*]) of the luminescence of firefly luciferase "relative" to the luminescence of *Renilla* luciferase as means ± SEM, n = 3.

See also Figure S3 and Table S4.

that GO analysis for temporal HTVs can provide the functional landscape for HCMV miRNAs.

HTV Targets Associated with Cell Cycle, Apoptosis, and Autophagy

To assess whether genes involved in the biological pathways important for HCMV are functionally relevant, we analyzed several HTV targets that are associated with cell cycle, apoptosis, and autophagy. In cell-cycle regulation, we focused on *CCND1* and *CDK6* as HTV targets (Figure S5A and Table S3), which has been studied more intensively than that of other cell-cycle checkpoint genes in HCMV infection and associated with pseudo-G1 phase establishment in HCMV-infected cells (Sanchez and Spector, 2008). We also identified *FAS*, *FADD*, *CASP2*, *CASP3*, and *CASP7*, which are related to the apoptosis signaling pathway (Figure S5B and Table S3), and *ULK1*, *ULK2*, *ATG2B*, *ATG5*, *ATG9A*, *ATG12*, *ATG13*, *ATG16L1*, *GABARAP*, *GABARAPL2*, and *MAP1LC3B*, which are associated with autophagy inhibition (Figure S5C and Table S3). We found that the mRNA levels of these HTV target genes were reduced upon transfection of corresponding viral miRNA mimics in HFFs (Figures 5A and S5D) and further verified by luciferase reporter assays for the 3′ UTRs of target mRNAs (Figure 5B), validating that these HTV targets are authentic targets of HCMV miRNAs. We also observed the protein downregulation of some of these genes tested (Figure 5C).

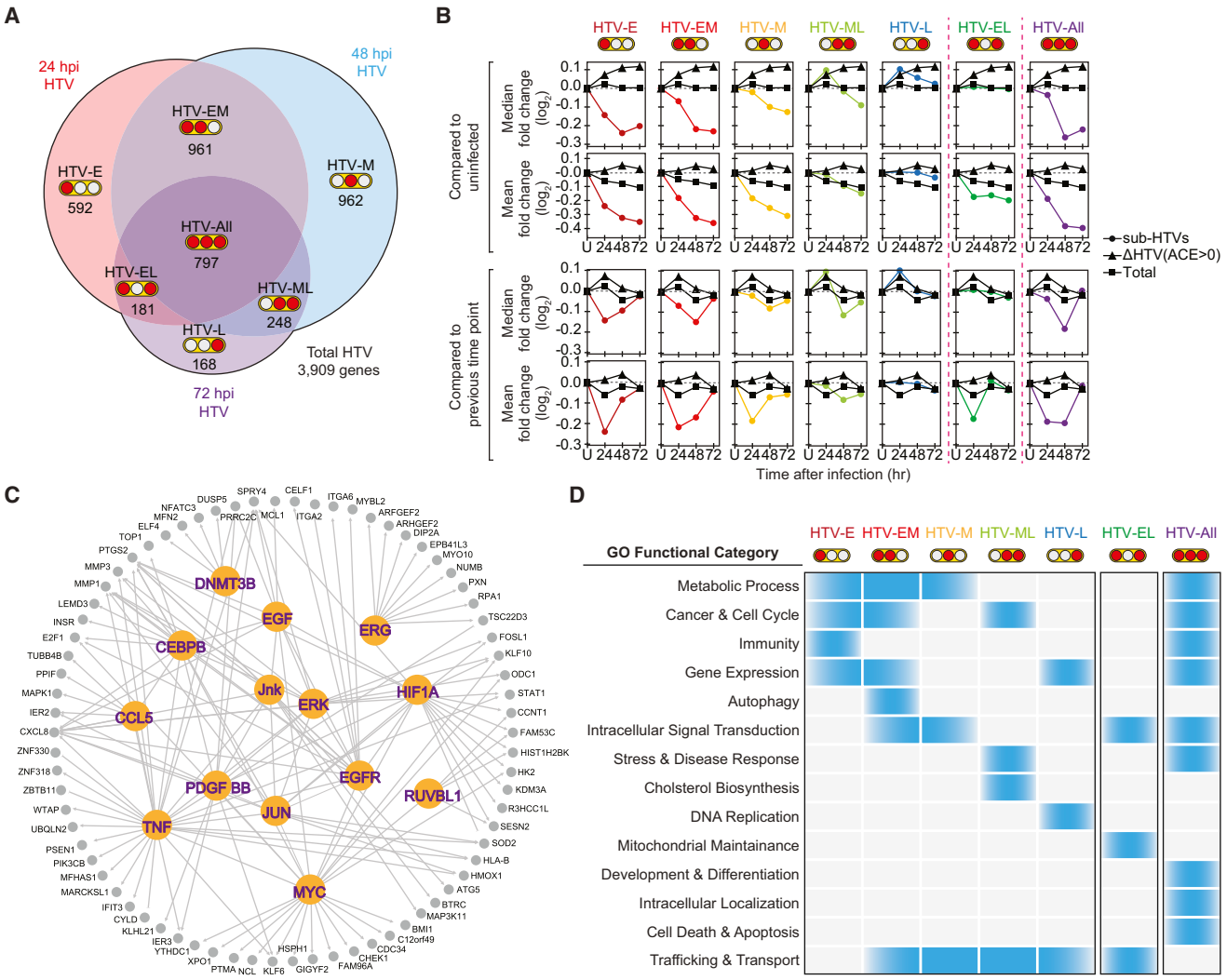

Figure 4. Emergent Property and Functional Landscape of Sub-temporal HTVs

(A) Venn diagram of seven sub-temporal HTVs. Sub-temporal HTV names are indicated as bold characters. Graphical symbols and the number of target genes (ACE-score > 0) for sub-temporal HTVs are shown below the names. Red dots in three circles indicate the representing periods of sub-temporal HTVs.

(B) Median and mean fold changes of sub-temporal HTVs at the transcriptome level. Upper panels: fold changes compared to previous time point. Lower panels: fold changes compared to uninfected time point.

(C) Upstream analysis for 72 hpi HTV targets. 72 hpi HTV genes were subjected to upstream analysis using IPA (www.ingenuity.com). Several 72 hpi HTV genes were clustered by central nodes of 14 main activator genes, which are indicated by enlarged purple characters. Arrows represent activation or induction direction to downstream target genes.

(D) Summary of representative GO categories. GO analysis and functional clustering were performed using ClueGO plugin in Cytoscape program. Blue boxes indicate significantly enriched representation of GO categories in those sub-temporal HTVs.

See also Figure S4 and Tables S5 and S6.

We observed that HFFs transfected with HCMV miRNAs exhibited a suppressive effect on cell-cycle progression, such as inducing G1 arrest (Figures 5D and S5E), further strengthening the physiological significances. Moreover, we found that a mixture of HCMV miRNAs downregulated FAS-mediated apoptosis compared to non-targeting control miRNAs using a lactate dehydrogenase (LDH) release assay (Figure 5E). In regards to viral miRNA-mediated regulation of the autophagosome formation, the number of autophagic GFP-LC3 puncta induced by serum starvation was lower in viral miRNA-transfected cells than in control miRNA-transfected cells (Figure 5F). Therefore, we concluded that HCMV miRNAs collectively target various cellular mRNAs to establish the pseudo-G1 phase, regulate apoptotic signaling ensuring its survival, and inhibit the formation of autophagosomes.

Modulation of Interferon JAK/STAT Signaling Pathway through miRNA-Mediated HTV Suppression

Viruses counteract the interferon (IFN) signaling pathway with viral proteins immediately after infection and throughout the course of infection. The specific mechanisms used by HCMV to evade IFN responses have been primarily studied with

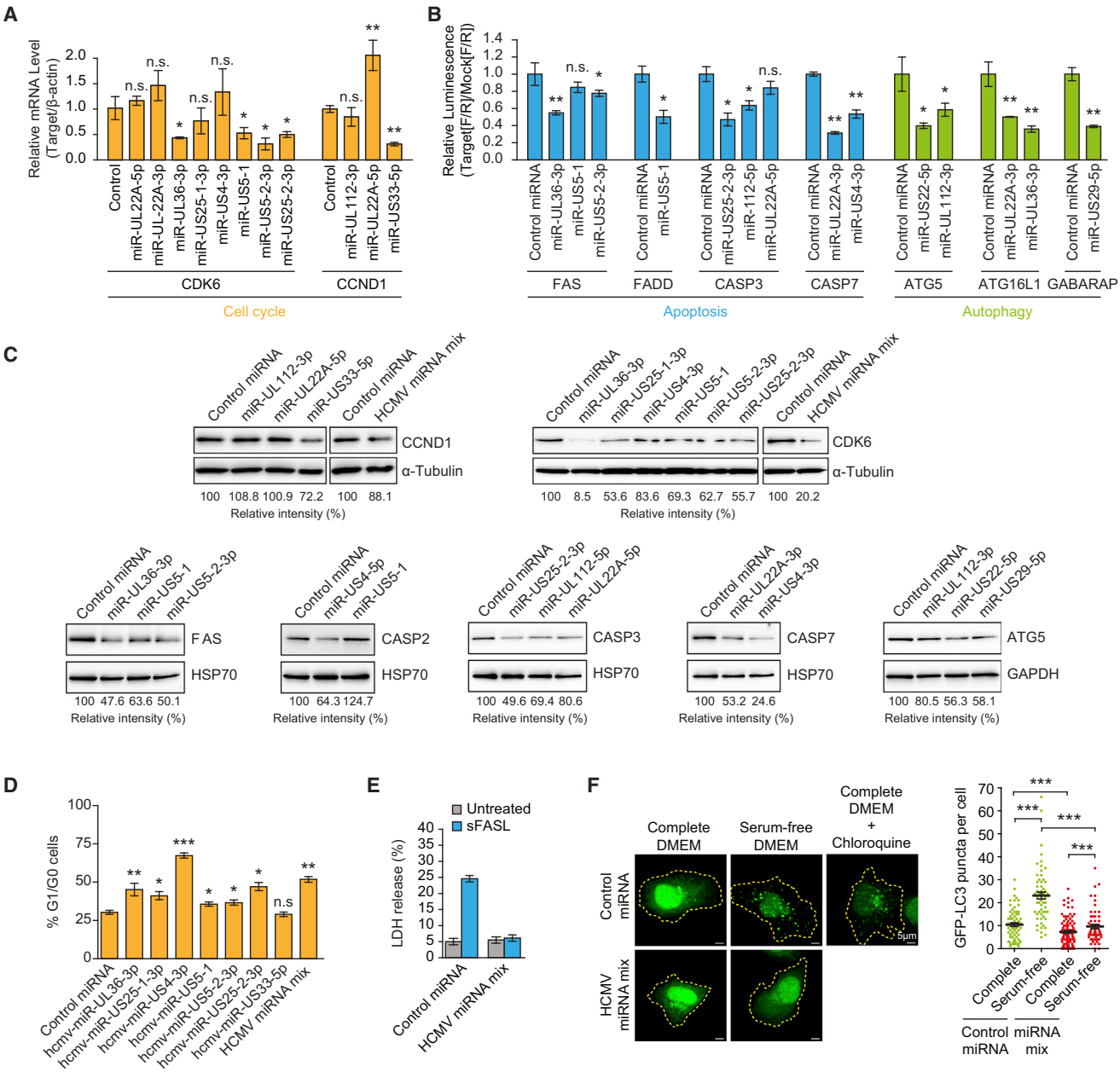

Figure 5. Functional Validation of HTV Targets Related to Cell Cycle and Apoptosis

(A) Relative fold changes of CDK6 and CCND1 mRNAs in HFFs transfected with the corresponding HCMV miRNAs. The expression levels of target mRNAs were analyzed using qRT-PCR. *$p < 0.05$, **$p < 0.01$, bootstrapped t test with 10,000 repetitions, compared with control miRNA. Data are presented relative to the value of β-actin as means ± SEM, n = 3.

(B) Dual luciferase assay of relative luminescence of firefly luciferase with FAS, FADD, CASP3, CASP7, ATG5, ATG16L2, and GABARAP 3′ UTRs with the corresponding HCMV miRNAs. Dual luciferase assays were performed in HEK293T cells under the same condition as that in Figure 3B. *$p < 0.05$, **$p < 0.01$, bootstrapped t test with 10,000 repetitions, compared with control miRNA. Data are presented by dual normalization of the luminescence of firefly luciferase relative to the luminescence of *Renilla* luciferase as means ± SEM, n = 3.

(C) Immunoblots of CCND1, CDK6, FAS, CASP2, CASP3, CASP7, and ATG5 in HFFs transfected with the corresponding HCMV miRNAs. HCMV miRNA mixes were mixtures of hcmv-miR-UL112-3p, -UL22A-5p, and -US33-5p in CCND1 immunoblots and hcmv-miR-UL36-3p, -US25-1-3p, -US5-1, -US5-2-3p, and -US25-2-3p in CDK6 immunoblots. Anti-ATG5 antibody was used to detect ATG5-ATG12 conjugates. Alpha-tubulin (α-Tubulin), heat shock protein 70 (HSP70), and glyceraldehyde 3-phosphate dehydrogenase (GAPDH) served as the protein loading control.

(D) Frequency alteration of G1/G0-arrested cells by HCMV miRNAs. HFF cells were transfected with the synthetic miRNA mimics indicated. After 48 hr, 100 ng/ml of nocodazole were treated and incubated for 24 hr. PI stained cells were then analyzed by flow cytometry. *$p < 0.05$, **$p < 0.01$, ***$p < 0.001$, bootstrapped t test with 10,000 repetitions, compared with control miRNA. Data are presented as means ± SEM, n = 3.

(legend continued on next page)

respect to IE1 protein function mediated by the interaction between STAT1 and STAT2, which relocalize into PML bodies (Amsler et al., 2013). Although the disruption of type I and II IFN signaling can be explained solely by IE1 activity, all of the mechanisms by which the protein levels of IFNAR1, IFNAR2, JAK1, STAT1, and STAT2 are reduced during HCMV infection (Weekes et al., 2014) have not been completely elucidated. Thus, we aimed to identify the targets in HTV that are associated with the IFN JAK/STAT pathways. *IFNAR1*, *IFNAR2*, *IFNGR2*, *JAK1*, *JAK2*, *STAT1*, *STAT2*, and *IL10R2* were predicted to be HTV targets (Figure 6A and Table S3). We validated the functionality of the targeting interactions using luciferase reporter assays (Figure 6B) and qRT-PCR for transcripts (Figure S6A). The reductions in STAT1 and STAT2 protein expression by the corresponding viral miRNAs were confirmed by immunoblotting (Figure 6C). To access the functionality of viral miRNAs in IFN signaling pathways, we examined whether IFN-stimulated genes (ISGs) were induced in HFFs by type I IFN-β or type II IFN-γ treatment with or without viral miRNA transfection. ISG induction was inhibited by viral miRNA transfection after either IFN-β (Figures 6D and S6B) or IFN-γ treatment (Figures 6E and S6C), except in the case of miR-UL112-3p.

To validate the physiological relevance under conditions of HCMV infection, we pre-treated HFFs with either mixed viral miRNA mimics or anti-microRNA oligonucleotide (AMO) inhibitors. At 6 hr after transfection, the cells were infected with HCMV for 48 hr, and the induction of ISGs in response to type I IFN-β or type II IFN-γ treatment was determined. The AMO-mediated inhibition of viral miRNA expression and function had a de-suppressive effect on IFN-signaling-related targets of HCMV miRNAs during infection (Figures 6F and S6D), while the miRNA mimics had an enhancing effect for their signaling suppression (Figures 6G and S6E). Taken together, these results indicated that HCMV can inhibit IFN JAK/STAT signaling pathways by expressing miRNAs in addition to viral proteins and suggested a mechanism for the regulation of IFN signaling during HCMV infection.

Co-targeting and Cooperativity between HCMV and Human miRNA Targetomes

We aimed to identify the targetomes of human miRNAs that were dramatically increased or decreased during HCMV infection. With 299 human miRNAs expressed at a meaningful level, which have AGO-CLIP-seq RPM (reads per million reads) values of >50 at least at once in the four time points, we found 39 increased human miRNAs and 25 decreased human miRNAs (Figure 7A), of which the fold changes were highly correlated between small-RNA-seq and AGO-CLIP-seq (Figure 7B). Using our ACE-score-based method, canonical human 3′ UTR targets of upregulated human miRNAs (HTI, human targetome of increased human miRNAs) and downregulated human miRNAs (HTD, human targetome of decreased human miRNAs) were defined by ACE-score cut-off of >1 and <−1, respectively. We found that the overall mRNA expression of HTI targets, but not of HTD targets, gradually decreased after infection (Figure 7C). Also, the expression of the majority of the individual HTI targets significantly decreased, whereas the HTD targets were not increased (Figure 7D).

Here, we hypothesized that the increased target repression activity of human miRNAs that were upregulated after infection would be potentiated by co-targeting with HCMV miRNAs, whereas weakened target de-repression effects of downregulated human miRNAs would be a consequence of target sharing with HTV targets. To address these issues, we investigated the target overlap between HTV targets and HTI targets and found that approximately 86% (2,770/3,202) of HTV targets (ACE-score > 1) were shared with approximately 58% (2,770/4,772) of HTI targets (ACE-score > 1) (Figure 7E). Overlapping targets (Overlap) showed the greatest suppression, whereas non-overlapping HTV and HTI targets (HTV-only and HTI-only, respectively) exhibited relatively moderate downregulation (Figure 7F). The relative suppression efficiency of HTI was slightly greater than that of HTV, indicating that sharing targets with HTI might intensify the suppression of most HTV targets.

Next, to elucidate the functional aspects of HCMV miRNA-specific HTVs (Table S7), we performed GO analysis and network clustering of enriched terms using ClueGO for 432 HTV-only targets (Figure S7). Terms associated with "nuclear division" and "cell cycle" as well as "processing of protein and RNA" are significantly enriched, suggesting that the functionality of HCMV miRNA-specific targeting itself might be physiologically relevant in regards to cell-cycle arrest, the regulation of host gene production, and the enhancement of viral gene production and assembly.

We also compared HTV targets with HTD targets and identified relatively a few (214) HTD targets with an ACE-score < −1 (Figure 7G). The fold changes of HTV-only targets (ACE-score > 1, approximately 95%, 3,043/3,202) were similar to those of all HTV targets (Figure 7H, compared to Figure 2D), whereas HTD-only targets (ACE-score < −1, approximately 26%, 55/214) were upregulated due to de-repression as a result of downregulated human miRNAs. Overlapping targets (159 targets) were only slightly regulated, suggesting a potential combined effect of both repression by HTVs and de-repression by HTDs. Thus, the overall inefficient de-repression activity of HTDs might result from sharing the majority of HTD targets (approximately 74%, 159/214) with HTVs, indicating that by co-targeting with viral miRNAs during HCMV infection, target de-repression due to downregulated miRNAs is less significant than the potentiated suppression of increased miRNAs.

(E) Lactate dehydrogenase (LDH) release assay in HeLa cells transfected with the indicated HCMV miRNA mixture without or with recombinant soluble FAS ligand (sFASL) treatment. Minimum and maximum releases of LDH from transfected/untreated HFFs are indicated as percentages (0%–100%). Relative release of LDH from experimental cells was calculated and shown in the graph as means ± SEM, n = 3.

(F) Representative images (bar, 5 μm) and the number of GFP-LC3 positive puncta per cell in HeLa cells transfected with control or HCMV miRNAs. Autophagy was induced by cultivation of cells in serum-free DMEM for 6 hr or treatment with chloroquine at 100 μM for 6 hr as an inducer of autophagosome formation. Between 50 and 100 cells were analyzed per assay. ***p < 0.001, Poisson GLM tests.

See also Figure S5.

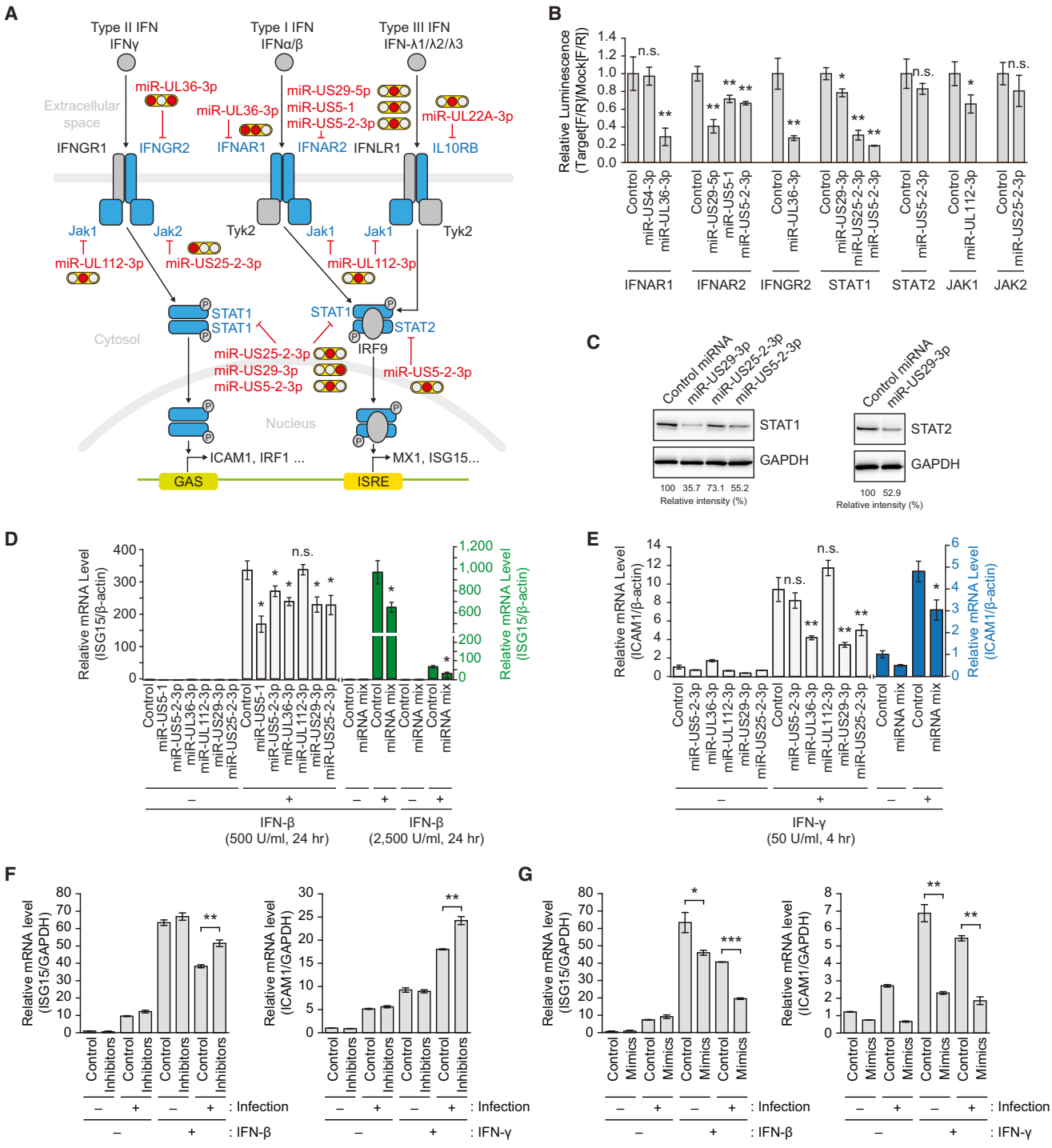

Figure 6. Physiological Relevance of HTV Targets Associated with IFN Signaling Pathway

(A) Schematic depiction of interferon (IFN) JAK-STAT pathway with HTV targets.

(B) Dual luciferase assay of relative luminescence of firefly luciferase with IFNAR1, IFNAR2, IFNGR2, STAT1, STAT2, JAK1, and JAK2 3′ UTRs with the corresponding HCMV miRNAs. *$p < 0.05$, **$p < 0.01$, bootstrapped t test with 10,000 repetitions, compared with control miRNA. Data are presented by dual normalization of the luminescence of firefly luciferase relative to the luminescence of *Renilla* luciferase as means ± SEM, n = 3.

(C) Immunoblots of STAT1 and STAT2 proteins in HFFs transfected with the corresponding HCMV miRNAs. GAPDH was served as the protein loading control.

(D and E) Relative levels of ISG15 (D) and ICAM1 (E) mRNA induced by IFN-β (D) or IFN-γ (E) treatment of HFFs transfected with control or HCMV miRNAs. 500 U/ml or 2,500 U/ml of IFN-β (PeproTech) were treated for 24 hr, and 50 U/ml of IFN-γ (PeproTech) was treated for 4 hr.

(F and G) Relative levels of ISG mRNAs induced by IFN-β or IFN-γ treatment of uninfected or HCMV-infected HFFs transfected with inhibitors or mimic mixtures of control or HCMV miRNAs. Before 6 hr of HCMV infection, control inhibitor or mixed ZEN modified 2′-O-methyl AMO inhibitors for HCMV miRNAs (F), and control

(legend continued on next page)

DISCUSSION

In this study, we applied genome-wide comparative analysis to AGO-CLIP-seq data from HCMV-infected cells and uninfected cells. Our analysis in the context of dynamic infection is a pioneering approach for AGO-CLIP-seq-based miRNA targetomics that is distinct from most previous studies performed in homotypic cells or heterogeneous tissue samples without comparative controls. The inclusion of the uninfected control in our AGO-CLIP-seq analysis improved the accuracy of authentic target site identification for viral or human miRNAs and enabled us to elucidate physiologically significant changes during HCMV infection using our ACE-scoring method.

Several previous studies have already shown that most viral miRNAs have functions similar to those of viral proteins by co-targeting common pathways or cellular processes for viral benefit (Jackson et al., 2011; Kim et al., 2011; Lee et al., 2012; Stern-Ginossar et al., 2007). In this study, we validated many genes related to cell cycle, apoptosis, autophagy, and IFN signaling pathways, which were represented as HTV targets that have been previously studied in the context of protein-coding viral gene-mediated regulation. In the pseudo-G1 state, the steady-state mRNA and protein levels of S-cyclin A and G1-cyclin D1 are diminished. Although viral processes are mediated mainly by pUL69 and pp71 immediately following infection and subsequently by IE1/IE2 and UL37 IE RNA during the early phase (Sanchez and Spector, 2008), viral miRNAs can also help prolong the pseudo-G1 state. To suppress the apoptosis of infected cells, HCMV encodes multiple apoptosis inhibitors, such as UL36, UL37, IE1, IE2, UL38, and non-coding RNA β2.7 (McCormick, 2008). FAS downregulation in HCMV-infected cells has been reported at the late phase of infection with lack of precise mechanism study (Seirafian et al., 2014). It might be partly explained by the viral miRNA-mediated mechanism uncovered previously. HCMV has been also reported to induce autophagy at the very early phase of infection and to inhibit autophagosome formation by viral gene expression during the later phase of infection, which was characterized in part by investigating HCMV TRS1 protein function (Chaumorcel et al., 2012). Although distinct domains of TRS1 interact with Beclin and affected by TRS1 deletion, we additionally showed that autophagy inhibition at the later phase of HCMV infection can be affected by HCMV-encoded miRNAs. Thus, our results support the idea that viruses execute redundant strategies to regulate host cellular processes by using their protein coding genes and non-coding RNA, including miRNAs, collectively.

Virus infection can affect host miRNA expression and function through either direct regulation of viral gene products or the host anti-viral response. This prompted us to examine whether dynamically upregulated human miRNAs can cooperate with HCMV miRNAs by sharing common targets or targeting common molecular pathways and whether target de-repression of downregulated human miRNAs might be diminished by sharing targets with viral miRNAs. Interestingly, we found that a large fraction of human miRNA targets were shared with viral miRNAs, and the targeting efficiency of upregulated human miRNAs was more suppressed, whereas the targetome of downregulated human miRNAs was not sufficiently de-repressed, indicating that viral miRNAs might utilize the targeting ability of host miRNAs to regulate their target selection. However, evolutionary conservation of targetome sharing between viral and host miRNAs remains to be studied.

Because virally encoded miRNAs are non-immunogenic, unlike viral proteins that can elicit strong immune responses, it was not too surprising that HCMV, which is a master of immune evasion, uniquely developed its miRNAs to escape both host innate and adaptive immune responses. Most HCMV miRNAs are expressed and function in latently infected cells (Shen et al., 2014), indicating that treatments against the expression and function of viral miRNAs have a potential to affect the establishment of latent infection. Despite numerous efforts for over 30 years to develop HCMV vaccines that target viral proteins, no vaccine appears to be approaching imminent licensure (Dasari et al., 2013; Schleiss, 2008). Thus, our targetome data could be used to identify novel drug targets and to improve our understanding of HCMV virology.

To understand cellular processes in lytic HCMV-infected cells, comprehensive genome-wide approaches should be used in an unbiased manner. Recent genome-wide studies of ribosomal profiling and quantitative proteomics are good examples in the context of productive HCMV infection (Stern-Ginossar et al., 2012; Weekes et al., 2014). Therefore, together with these studies that employed large-scale screening of translated open reading frames and temporal alteration of viral proteomes, our study characterizing temporal miRNA targetomes in productive HCMV-infected cells is an invaluable resource for establishing a holistic perspective on host-virus interactions.

EXPERIMENTAL PROCEDURES

A full description of Experimental Procedures is available in the Supplemental Information.

Cell Lines

HFFs, HEK293T cells, and HeLa cells were obtained from the American Type Culture Collection and cultured in complete DMEM (Hyclone) supplemented with 10% FBS (Hyclone), 2 mM GlutaMAX-I (Gibco), 100 U/ml penicillin (Invitrogen), and 100 μg/ml streptomycin (Invitrogen) at 37°C in the presence of 5% CO_2. To arrest cell-cycle progression at the pseudo-metaphase, 100 ng/ml of nocodazole were treated and incubated for 24 hr.

HCMV Infection

HFF cells were trypsinized, resuspended, and plated at near confluence. All infections were performed with the HCMV $Towne_{long}$ strain (Bradley et al., 2009) at multiplicity of infection (moi) = 3 and with five immunofluorescence units (IFU) per cell. DMEM without serum was used for mock infections. After virus absorption for 1 hr, virus-containing medium was immediately replaced by complete DMEM. Cells were harvested at the indicated post-infection times after washing with PBS twice.

miRNA or HCMV miRNA mimic mixture (G) were transfected in HFF cells for 6 hr and then infected without or with HCMV at 1 moi. After 48 hr, by qRT-PCR, we quantified the relative levels of ISG15 and ICAM1 mRNA induced by IFN-β or IFN-γ treatment for 16 hr, respectively.
(D–G) The expression levels of target mRNAs were analyzed using qRT-PCR. *$p < 0.05$, **$p < 0.01$, bootstrapped t test with 10,000 repetitions, compared with control miRNA. Data are presented relative to the value of β-actin as means ± SEM, n = 3.
See also Figure S6.

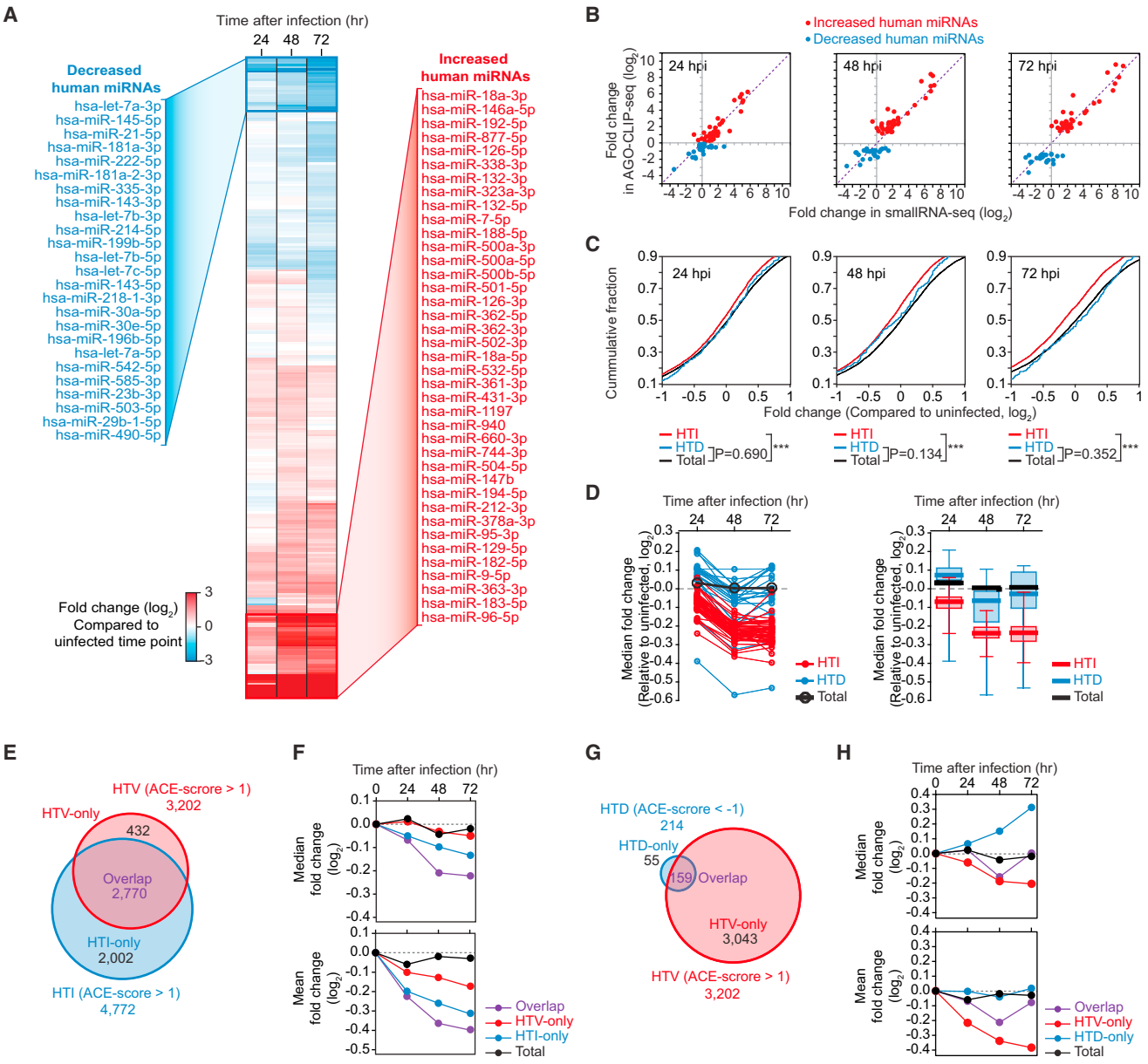

Figure 7. Characterization of the Targetomes of Human miRNAs Dynamically Changed during HCMV Infection

(A) Hierarchical cluster heatmap of fold changes (log_2) of highly AGO-loaded human miRNAs with >50 RPM (reads per million) in AGO-CLIP-seq data during HCMV infection. Increased human miRNAs are highlighted and listed in red. Decreased human miRNAs are highlighted and listed in blue.

(B) Correlation between fold changes (log_2) of increased or decreased human miRNAs indicated in (A) in smallRNA-seq and AGO-CLIP-seq. Data are compared to RPM values of uninfected samples and averages of duplicate smallRNA-seq and triplicate AGO-CLIP-seq.

(C) Cumulative fractions for mRNA expression fold change of increased human miRNAs (HTI) and decreased human miRNAs (HTD) at specified times. ***$p < 0.001$, two-sample Kolmogorov-Smirnov test (2-sided).

(D) Fold changes of targets of individual HTIs and HTDs. Left: data are displayed as median fold changes (log_2, relative to uninfected RPKM). Right: data from the left panel are replotted with indicators: whiskers (min/max), boxes (10%–90%), bold bar (mean).

(E) Venn diagram of HTV (ACE-score > 1, red) and HTI (ACE-score > 1, blue). The numbers of target genes in each region are shown.

(F) Median fold changes (log_2) of overlap of HTV and HTI (purple), only HTV (red), only HTI (blue), and total genes (black). Data are given as values compared to uninfected.

(G) Venn diagram of HTV (ACE-score > 1, red) and HTD (ACE-score < −1, blue). The numbers of target genes in each region are shown.

(H) Median fold changes (log_2) of overlap of HTV and HTD (purple), only HTV (red), only HTD (blue), and total genes (black). Data are given as values compared to uninfected.

See also Figure S7 and Table S7.

Luciferase Reporter Assay

HEK293T cells were seeded in 24-well plates 1 day before transfection. For co-transfection, 5 ng firefly luciferase and 2.5 ng *Renilla* luciferase reporter plasmids were transiently transfected into cells with 20 pmol of miRNA artificial oligomer (synthesized and annealed by Bioneer). After 24–48 hr, luciferase activity was measured with a Dual Luciferase Reporter Assay System (Promega).

Immunoblotting

Cells were lysed for 1 hr at 4°C with 1% (v/v) Nonidet P-40 (NP-40) or RIPA buffer in PBS with a protease-inhibitor cocktail, separated on a 4%–12% NuPAGE Bis-Tris gel (NP0321BOX, Invitrogen) according to the manufacturer's instructions using 800 ml of 1× MOPS running buffer (NP0001, Invitrogen), transferred onto nitrocellulose membranes with NuPAGE Transfer Buffer (NP00061, Invitrogen), blocked with 3% BSA in Tris-buffered saline with 0.1% Tween 20 (0.1% TBST), and probed overnight with the appropriate antibodies in 0.1% TBST. Membranes were washed with 0.1% TBST, incubated for 1 hr with horseradish peroxidase-conjugated secondary antibody (Jackson ImmunoResearch Laboratories), and finally washed with 0.1% TBST. Proteins on immunoblots were visualized with ECL Western Blotting Substrate (Thermo Scientific Pierce).

Lactate Dehydrogenase Release Assay

HFFs were transfected with control or HCMV miRNA oligomers for 48 hr before treatment with or without 100 ng/ml recombinant human soluble FAS ligand (sFASL; PeproTech, 310-03H) and harvested at 12 hr after sFASL treatment. The LDH release assay was performed using an LDH Cytotoxicity Detection Kit (Clontech, 630117) according to the manufacturer's protocol.

Statistical Analysis

Statistical comparisons for cumulative relative frequency (fraction) were conducted using the Kolmogorov-Smirnov test (K-S test) with XLSTAT software. In the K-S test, p values $\leq$ 0.0001 (*) were considered statistically significant. Statistical comparisons for continuous variables were conducted using bootstrapped t tests with 10,000 repetitions (Neuhäuser and Jöckel, 2006). To compare discrete random variables, a Poisson generalized linear model was applied to determine statistical significance. All data are shown as means ± SEM. We conducted bootstrapped t test with in-house software and used R statistical software (v. 3.0.1) for all other comparisons. p values $\leq$ 0.05 (*), 0.01 (**), and 0.001 (***) were considered statistically significant.

ACCESSION NUMBERS

The data files of all replicates of AGO-CLIP-seq, mRNA-seq, and smallRNA-seq were deposited under NCBI GEO accession number GSE63797.

SUPPLEMENTAL INFORMATION

Supplemental Information includes Supplemental Experimental Procedures, seven figures, and seven tables and can be found with this article online at http://dx.doi.org/10.1016/j.chom.2015.05.014.

AUTHOR CONTRIBUTIONS

S.K. and K.A. designed the experimental strategies. S.K., D.K., Y.H., and S.L. performed the experiments. D.S., H.C., D.B., and V.N.K. performed bioinformatic analysis of the sequence data. S.K., D.S., and K.A. wrote the manuscript. K.A. supervised all research. All authors contributed to discussion about the data.

ACKNOWLEDGMENTS

The authors would like to thank Jin-Hyun Ahn and Young-Eui Kim for providing HCMV $Towne_{long}$ and the laboratory members of V. Narry Kim and Kwangseog Ahn for their helpful discussions and technical assistance. This work was supported by the Creative Research Initiative Program (Research Center for Antigen Presentation, 2006-0050689), Global Ph.D. Fellowship Program through the National Research Foundation of Korea (NRF) funded by the Ministry of Education (2012-015863) (Y.H.), the BK21 Research Fellowships from the Ministry of Education of Korea (Y.H.), IBS-R008-D1 of Institute for Basic Science from the Ministry of Science, ICT and Future Planning of Korea (V.N.K., D.B., and K.A.), and the Korean Basic Science Research Program (2011-0014523) from the NRF funded through the Ministry of Education, Science, and Technology (MEST) of Korea (D.B.).

Received: January 12, 2015
Revised: April 16, 2015
Accepted: May 18, 2015
Published: June 10, 2015

REFERENCES

Amsler, L., Verweij, M.C., and DeFilippis, V.R. (2013). The tiers and dimensions of evasion of the type I interferon response by human cytomegalovirus. J. Mol. Biol. *425*, 4857–4871.

Bailey, T.L., and Elkan, C. (1994). Fitting a mixture model by expectation maximization to discover motifs in biopolymers. Proc. Int. Conf. Intell. Syst. Mol. Biol. *2*, 28–36.

Bindea, G., Mlecnik, B., Hackl, H., Charoentong, P., Tosolini, M., Kirilovsky, A., Fridman, W.H., Pagès, F., Trajanoski, Z., and Galon, J. (2009). ClueGO: a Cytoscape plug-in to decipher functionally grouped gene ontology and pathway annotation networks. Bioinformatics *25*, 1091–1093.

Boldogh, I., AbuBakar, S., Deng, C.Z., and Albrecht, T. (1991). Transcriptional activation of cellular oncogenes fos, jun, and myc by human cytomegalovirus. J. Virol. *65*, 1568–1571.

Boudreau, R.L., Jiang, P., Gilmore, B.L., Spengler, R.M., Tirabassi, R., Nelson, J.A., Ross, C.A., Xing, Y., and Davidson, B.L. (2014). Transcriptome-wide discovery of microRNA binding sites in human brain. Neuron *81*, 294–305.

Bradley, A.J., Lurain, N.S., Ghazal, P., Trivedi, U., Cunningham, C., Baluchova, K., Gatherer, D., Wilkinson, G.W., Dargan, D.J., and Davison, A.J. (2009). High-throughput sequence analysis of variants of human cytomegalovirus strains Towne and AD169. J. Gen. Virol. *90*, 2375–2380.

Chaumorcel, M., Lussignol, M., Mouna, L., Cavignac, Y., Fahie, K., Cotte-Laffitte, J., Geballe, A., Brune, W., Beau, I., Codogno, P., and Esclatine, A. (2012). The human cytomegalovirus protein TRS1 inhibits autophagy via its interaction with Beclin 1. J. Virol. *86*, 2571–2584.

Chi, S.W., Zang, J.B., Mele, A., and Darnell, R.B. (2009). Argonaute HITS-CLIP decodes microRNA-mRNA interaction maps. Nature *460*, 479–486.

Dasari, V., Smith, C., and Khanna, R. (2013). Recent advances in designing an effective vaccine to prevent cytomegalovirus-associated clinical diseases. Expert Rev. Vaccines *12*, 661–676.

Fabian, M.R., Sonenberg, N., and Filipowicz, W. (2010). Regulation of mRNA translation and stability by microRNAs. Annu. Rev. Biochem. *79*, 351–379.

Garcia, D.M., Baek, D., Shin, C., Bell, G.W., Grimson, A., and Bartel, D.P. (2011). Weak seed-pairing stability and high target-site abundance decrease the proficiency of lsy-6 and other microRNAs. Nat. Struct. Mol. Biol. *18*, 1139–1146.

Gottwein, E., Corcoran, D.L., Mukherjee, N., Skalsky, R.L., Hafner, M., Nusbaum, J.D., Shamulailatpam, P., Love, C.L., Dave, S.S., Tuschl, T., et al. (2011). Viral microRNA targetome of KSHV-infected primary effusion lymphoma cell lines. Cell Host Microbe *10*, 515–526.

Grimson, A., Farh, K.K., Johnston, W.K., Garrett-Engele, P., Lim, L.P., and Bartel, D.P. (2007). MicroRNA targeting specificity in mammals: determinants beyond seed pairing. Mol. Cell *27*, 91–105.

Haecker, I., Gay, L.A., Yang, Y., Hu, J., Morse, A.M., McIntyre, L.M., and Renne, R. (2012). Ago HITS-CLIP expands understanding of Kaposi's sarcoma-associated herpesvirus miRNA function in primary effusion lymphomas. PLoS Pathog. *8*, e1002884.

Hafner, M., Landthaler, M., Burger, L., Khorshid, M., Hausser, J., Berninger, P., Rothballer, A., Ascano, M., Jr., Jungkamp, A.C., Munschauer, M., et al. (2010). Transcriptome-wide identification of RNA-binding protein and microRNA target sites by PAR-CLIP. Cell *141*, 129–141.

Hook, L., Hancock, M., Landais, I., Grabski, R., Britt, W., and Nelson, J.A. (2014a). Cytomegalovirus microRNAs. Curr Opin Virol *7*, 40–46.

Hook, L.M., Grey, F., Grabski, R., Tirabassi, R., Doyle, T., Hancock, M., Landais, I., Jeng, S., McWeeney, S., Britt, W., and Nelson, J.A. (2014b). Cytomegalovirus miRNAs target secretory pathway genes to facilitate formation of the virion assembly compartment and reduce cytokine secretion. Cell Host Microbe *15*, 363–373.

Jackson, S.E., Mason, G.M., and Wills, M.R. (2011). Human cytomegalovirus immunity and immune evasion. Virus Res. *157*, 151–160.

Kapoor, A., Cai, H., Forman, M., He, R., Shamay, M., and Arav-Boger, R. (2012). Human cytomegalovirus inhibition by cardiac glycosides: evidence for involvement of the HERG gene. Antimicrob. Agents Chemother. *56*, 4891–4899.

Kim, S., Lee, S., Shin, J., Kim, Y., Evnouchidou, I., Kim, D., Kim, Y.K., Kim, Y.E., Ahn, J.H., Riddell, S.R., et al. (2011). Human cytomegalovirus microRNA miR-US4-1 inhibits CD8(+) T cell responses by targeting the aminopeptidase ERAP1. Nat. Immunol. *12*, 984–991.

Kincaid, R.P., and Sullivan, C.S. (2012). Virus-encoded microRNAs: an overview and a look to the future. PLoS Pathog. *8*, e1003018.

Lee, S.H., Kalejta, R.F., Kerry, J., Semmes, O.J., O'Connor, C.M., Khan, Z., Garcia, B.A., Shenk, T., and Murphy, E. (2012). BclAF1 restriction factor is neutralized by proteasomal degradation and microRNA repression during human cytomegalovirus infection. Proc. Natl. Acad. Sci. USA *109*, 9575–9580.

Leung, A.K., Young, A.G., Bhutkar, A., Zheng, G.X., Bosson, A.D., Nielsen, C.B., and Sharp, P.A. (2011). Genome-wide identification of Ago2 binding sites from mouse embryonic stem cells with and without mature microRNAs. Nat. Struct. Mol. Biol. *18*, 237–244.

McCormick, A.L. (2008). Control of apoptosis by human cytomegalovirus. Curr. Top. Microbiol. Immunol. *325*, 281–295.

McFarlane, S., Nicholl, M.J., Sutherland, J.S., and Preston, C.M. (2011). Interaction of the human cytomegalovirus particle with the host cell induces hypoxia-inducible factor 1 alpha. Virology *414*, 83–90.

Nelson, P.T., De Planell-Saguer, M., Lamprinaki, S., Kiriakidou, M., Zhang, P., O'Doherty, U., and Mourelatos, Z. (2007). A novel monoclonal antibody against human Argonaute proteins reveals unexpected characteristics of miRNAs in human blood cells. RNA *13*, 1787–1792.

Neuhäuser, M., and Jöckel, K.H. (2006). A bootstrap test for the analysis of microarray experiments with a very small number of replications. Appl. Bioinformatics *5*, 173–179.

Pfeffer, S., Zavolan, M., Grässer, F.A., Chien, M., Russo, J.J., Ju, J., John, B., Enright, A.J., Marks, D., Sander, C., and Tuschl, T. (2004). Identification of virus-encoded microRNAs. Science *304*, 734–736.

Riley, K.J., Rabinowitz, G.S., Yario, T.A., Luna, J.M., Darnell, R.B., and Steitz, J.A. (2012). EBV and human microRNAs co-target oncogenic and apoptotic viral and human genes during latency. EMBO J. *31*, 2207–2221.

Rodems, S.M., and Spector, D.H. (1998). Extracellular signal-regulated kinase activity is sustained early during human cytomegalovirus infection. J. Virol. *72*, 9173–9180.

Sanchez, V., and Spector, D.H. (2008). Subversion of cell cycle regulatory pathways. Curr. Top. Microbiol. Immunol. *325*, 243–262.

Schleiss, M.R. (2008). Cytomegalovirus vaccine development. Curr. Top. Microbiol. Immunol. *325*, 361–382.

Seirafian, S., Prod'homme, V., Sugrue, D., Davies, J., Fielding, C., Tomasec, P., and Wilkinson, G.W. (2014). Human cytomegalovirus suppresses Fas expression and function. J. Gen. Virol. *95*, 933–939.

Shen, Z.Z., Pan, X., Miao, L.F., Ye, H.Q., Chavanas, S., Davrinche, C., McVoy, M., and Luo, M.H. (2014). Comprehensive analysis of human cytomegalovirus microRNA expression during lytic and quiescent infection. PLoS ONE *9*, e88531.

Skalsky, R.L., Corcoran, D.L., Gottwein, E., Frank, C.L., Kang, D., Hafner, M., Nusbaum, J.D., Feederle, R., Delecluse, H.J., Luftig, M.A., et al. (2012). The viral and cellular microRNA targetome in lymphoblastoid cell lines. PLoS Pathog. *8*, e1002484.

Soroceanu, L., Akhavan, A., and Cobbs, C.S. (2008). Platelet-derived growth factor-alpha receptor activation is required for human cytomegalovirus infection. Nature *455*, 391–395.

Stark, T.J., Arnold, J.D., Spector, D.H., and Yeo, G.W. (2012). High-resolution profiling and analysis of viral and host small RNAs during human cytomegalovirus infection. J. Virol. *86*, 226–235.

Stern-Ginossar, N., Elefant, N., Zimmermann, A., Wolf, D.G., Saleh, N., Biton, M., Horwitz, E., Prokocimer, Z., Prichard, M., Hahn, G., et al. (2007). Host immune system gene targeting by a viral miRNA. Science *317*, 376–381.

Stern-Ginossar, N., Weisburd, B., Michalski, A., Le, V.T., Hein, M.Y., Huang, S.X., Ma, M., Shen, B., Qian, S.B., Hengel, H., et al. (2012). Decoding human cytomegalovirus. Science *338*, 1088–1093.

Thomson, D.W., Bracken, C.P., and Goodall, G.J. (2011). Experimental strategies for microRNA target identification. Nucleic Acids Res. *39*, 6845–6853.

Wang, X., Huong, S.M., Chiu, M.L., Raab-Traub, N., and Huang, E.S. (2003). Epidermal growth factor receptor is a cellular receptor for human cytomegalovirus. Nature *424*, 456–461.

Weekes, M.P., Tomasec, P., Huttlin, E.L., Fielding, C.A., Nusinow, D., Stanton, R.J., Wang, E.C., Aicheler, R., Murrell, I., Wilkinson, G.W., et al. (2014). Quantitative temporal viromics: an approach to investigate host-pathogen interaction. Cell *157*, 1460–1472.

Xuan, B., Qian, Z., Torigoi, E., and Yu, D. (2009). Human cytomegalovirus protein pUL38 induces ATF4 expression, inhibits persistent JNK phosphorylation, and suppresses endoplasmic reticulum stress-induced cell death. J. Virol. *83*, 3463–3474.

Yordy, B., Tal, M.C., Hayashi, K., Arojo, O., and Iwasaki, A. (2013). Autophagy and selective deployment of Atg proteins in antiviral defense. Int. Immunol. *25*, 1–10.

Zhang, C., and Darnell, R.B. (2011). Mapping in vivo protein-RNA interactions at single-nucleotide resolution from HITS-CLIP data. Nat. Biotechnol. *29*, 607–614.